DOI: 10.24352/UB.OVGU-2017-104 TECHNISCHE MECHANIK, 37, 2-5, (2017), 280 – 290
submitted: June 15, 2017

On the Importance of Frictional Energy Dissipation in the Prevention of Undesirable Self-Excited Vibrations in Gas Foil Bearing Rotor Systems

T. Leister, C. Baum, W. Seemann

In this contribution, a nonlinear and fully coupled fluid–structure–rotor interaction model of a gas foil bearing rotor system is presented. Aiming at the reduction of undesirable self-excited vibrations, many common bearing designs feature a compliant and slightly movable multi-part foil structure inside the lubrication gap. The present paper discusses the general impact of frictional energy dissipation within the foil structure by adding equivalent viscous damping to the widespread simple elastic foundation model. For the computational analysis, the PDEs describing the fluid pressure distribution and the foil structure deformation field are spatially discretized using finite difference schemes. After suitable nondimensionalization of the resulting system of nonlinear ODEs, a corresponding state-space representation is deduced. Using numerical simulation tools, the stability of equilibrium points and the occurrence of self-excited vibrations are addressed and possible bifurcation scenarios are discussed. Summing up all results, frictional energy dissipation proves to be of crucial importance with regard to the reduction or prevention of undesirable self-excited vibrations in gas foil bearing rotor systems.

1 Introduction and Motivation

Gas foil bearings (GFBs) are an upcoming and promising oil-free technology in modern high-speed rotating machinery. Relying on a thin gas film building up an aerodynamic, load-carrying lubrication wedge, such bearings are self-acting and do not require any external pressurization. Most notably, due to the absence of solid-to-solid contact between the airborne rotor journal and the bearing sleeve, excessively low wear and power loss can be achieved (Heshmat et al., 1983). During the last few decades, the potential of GFBs has been widely confirmed by a great number of successful applications in air cycle machines of commercial aircraft (Howard et al., 2007). Lately, in particular as a result of insurmountable speed, temperature, and weight limitations of conventional rolling-element bearings, novel concepts of oil-free turbochargers (Howard, 1999) and oil-free rotorcraft propulsion engines (Howard et al., 2010) are gaining more and more interest.

Most of the considered rotating machinery is supposed to reach and to maintain a stable operating point after completing the run-up. However, as a result of the highly nonlinear bearing forces induced by the pressurized fluid, the existing equilibrium points of GFB rotor systems tend to become unstable for higher rotational speeds. Subsequently, undesirable self-excited vibrations with comparatively large amplitudes may occur (Bonello and Pham, 2014; Hoffmann et al., 2014; Baum et al., 2015a). For this reason, many common bearing designs feature a compliant and slightly movable multi-part foil structure inside the lubrication gap. By dissipating a certain amount of energy via dry sliding friction mechanisms (Peng and Carpino, 1993; Howard et al., 2001), this countermeasure is supposed to reduce the vibrational amplitudes or, as the ultimate goal, to prevent the occurrence of self-excited vibrations in the first place.

In currently conducted research on GFBs, sophisticated models and reliable numerical tools are of major interest with regard to the complexity and costliness of experimental investigations. As the classical mathematical model, based on the assumption of a full fluid film lubrication regime, the fluid pressurization is usually described by the Reynolds equation for compressible ideal gases (Reynolds, 1886; Szeri, 2010). With regard to the foil structure, many recent publications discuss complex FE models with or without considering frictional effects (Le Lez et al., 2007; San Andrés and Kim, 2008). In most cases, however, such models do not capture the true coupled nature of fluid–structure–rotor interaction (Bou-Saïd et al., 2008; Bonello and Pham, 2014) and thus prove to be inapplicable when it comes to a transient analysis of the system's nonlinear dynamic response. The main objective of the present paper is a systematic investigation of the general impact of energy dissipation within the foil structure. To this effect, a nonlinear and fully coupled model considering equivalent viscous damping

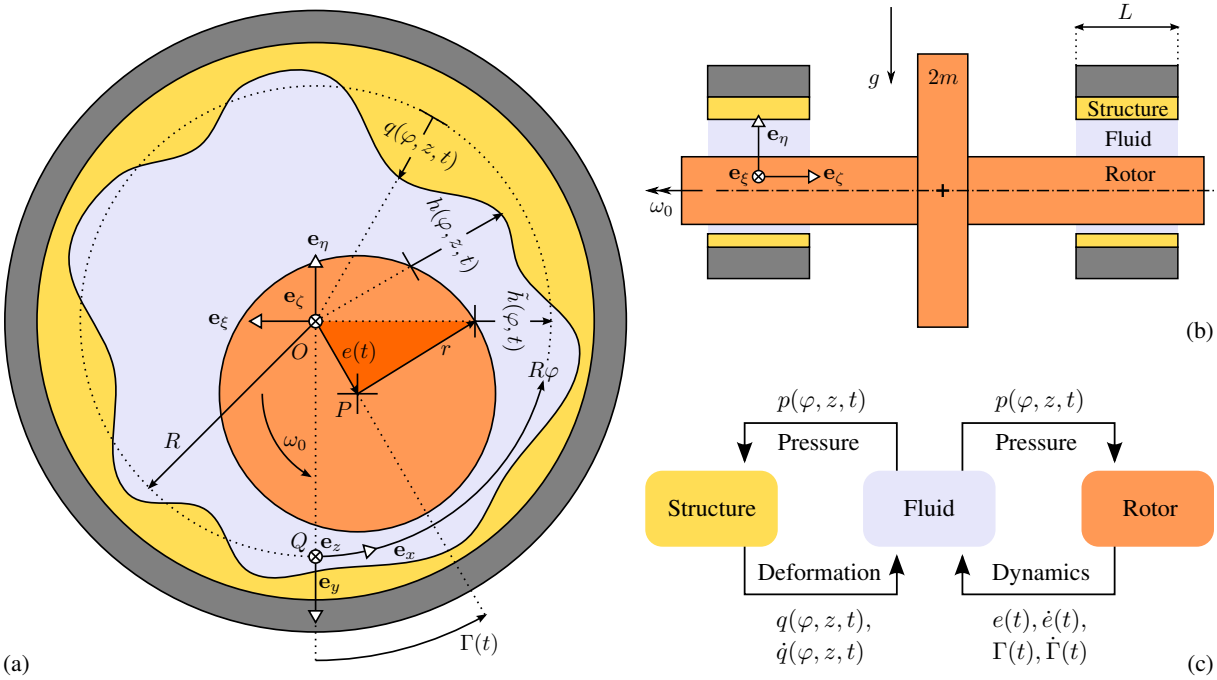

Figure 1. Schematic sketches (with greatly magnified lubrication gap) showing the fluid–structure–rotor model: (a) front view of the rotor journal inside the GFB model, (b) side view of the rotor model mounted on two GFBs, (c) interaction chart of the three fully coupled submodels.

is presented in a way which bears some basic resemblance to a recent contribution by Bonello and Pham (2014). Using numerical simulation tools, the essential question to be answered is whether and to what extent frictional energy dissipation is beneficial with regard to the reduction or prevention of undesirable self-excited vibrations.

2 Theory and Modeling

2.1 Fluid–Structure–Rotor Interaction

In the considered GFB rotor system, the pressurized fluid inside the lubrication gap is supposed to interact strongly with both the compliant foil structure and the movable rotor shaft (Bonello and Pham, 2014; Baum et al., 2015a; Leister et al., 2016a). In this regard, a realistic analysis of the system's nonlinear dynamic response requires an interconnected simulation approach in which all parts of the model are fully coupled to each other and in which all governing equations are solved simultaneously (Bonello and Pham, 2014; Baum et al., 2015a; Leister et al., 2016a). As depicted by the schematic sketches in Figure 1a (front view) and in Figure 1b (side view), the comprehensive overall model presented in this paper essentially comprises three submodels: an aerodynamic fluid model (colored in blue), a dissipative foil structure model (colored in yellow), and a turbomachine rotor model (colored in orange).

The basic bearing geometry is described by the axial length L of the bearing sleeve and by the inner radius R of the undeformed foil structure. Depending on the outer radius r of the rotor journal inside the bearing, the nominal height of the gas-filled lubrication gap is characterized in terms of a small radial clearance parameter

$$C = R - r, \qquad 0 < C/R \ll 1. \tag{1}$$

Given the small clearance assumption in Equation (1), the curvature of the lubrication gap and any radial dependence of the fluid properties can be neglected. Thus, the boundary value problem for the gas pressure calculation is henceforth considered on a two-dimensional, rectangular domain. Altogether, introducing a characteristic time scale T, we define a tuple of nondimensional independent variables $(\varphi, Z, \tau) = (x/R,\ z/L,\ t/T)$. The arising nondimensional time derivative is denoted by $(\square)' = \mathrm{d}(\square)/\mathrm{d}\tau$ for better legibility of the following equations.

The fluid–structure–rotor interaction chart in Figure 1c visualizes the coupling mechanisms between the three submodels. Defined in relation to the constant ambient pressure p_0, the nondimensional pressure field $P(\varphi, Z, \tau) = p(\varphi, ZL, \tau T)/p_0$ represents the load acting upon the foil structure. Moreover, the same pressure distribution induces

a bearing force which supports the rotor. On the other hand, the pressurization of the fluid is influenced by the dynamics of both the foil structure and the rotor. For this reason, considering the nominal radial clearance C from Equation (1), we introduce the nondimensional foil structure deformation field $Q(\varphi, Z, \tau) = q(\varphi, ZL, \tau T)/C$, the nondimensional rotor journal eccentricity $\varepsilon(\tau) = e(\tau T)/C$, and the nondimensional rotor journal attitude angle $\gamma(\tau) = \Gamma(\tau T)$. Due to squeeze effects which are discussed later, a transient coupling mechanism must also account for the respective time derivatives $Q'(\varphi, Z, \tau)$, $\varepsilon'(\tau)$, and $\gamma'(\tau)$.

2.2 Aerodynamic Fluid Model

It is obvious from the sketch in Figure 1a that the effective fluid film thickness $h(\varphi, z, t)$ depends on the nominal lubrication gap clearance, the foil structure deformation field, and the position of the rotor journal, which is assumed to be perfectly aligned with the bearing. By applying the law of cosines to the highlighted orange triangle and after linearization with respect to the rotor journal eccentricity, we find the nondimensional expression

$$H(\varphi, Z, \tau) = \frac{h(\varphi, ZL, \tau T)}{C} = \overbrace{1}^{\text{Clearance}} \quad \overbrace{-\varepsilon(\tau)\cos\Big[\varphi - \gamma(\tau)\Big]}^{\text{Rotor position}} \quad \overbrace{-Q(\varphi, Z, \tau)}^{\text{Structure deformation}} \tag{2}$$

and the corresponding nondimensional time derivative

$$H'(\varphi, Z, \tau) = -\varepsilon'(\tau)\cos\Big[\varphi - \gamma(\tau)\Big] - \varepsilon(\tau)\gamma'(\tau)\sin\Big[\varphi - \gamma(\tau)\Big] - Q'(\varphi, Z, \tau). \tag{3}$$

The considered bearing is supposed to operate within the full fluid film lubrication regime, such that a minimum fluid film thickness larger than the surrounding surface roughnesses is sustained at any time. In this case, the lubricant pressure is governed by a generalized form of the classical Reynolds equation which is applicable for compressible fluids (Reynolds, 1886; Szeri, 2010). Under isothermal conditions with a constant viscosity μ_0 and under the assumption of the ideal gas law, we obtain the nondimensional partial differential equation (PDE)

$$\left\{ \overbrace{P'}^{\text{Expansion}} \right\} H + P \left\{ \overbrace{-\varepsilon'(\tau)\cos\Big[\varphi - \gamma(\tau)\Big] - \varepsilon(\tau)\gamma'(\tau)\sin\Big[\varphi - \gamma(\tau)\Big]}^{\text{Rotor squeeze}} \quad \overbrace{-Q'}^{\text{Structure squeeze}} \right\}$$
$$= \frac{\partial}{\partial\tau}\Big[PH\Big] = \frac{1}{2}\left\{ \underbrace{\frac{\partial}{\partial\varphi}\left[PH^3\frac{\partial P}{\partial\varphi}\right] + \kappa^2\frac{\partial}{\partial Z}\left[PH^3\frac{\partial P}{\partial Z}\right]}_{\text{Poiseuille}} \quad \underbrace{-\Lambda\frac{\partial}{\partial\varphi}\Big[PH\Big]}_{\text{Couette}} \right\}, \tag{4}$$

which involves the fluid film thickness from Equation (2) and the corresponding time derivative from Equation (3). In the above stated PDE, a nondimensional bearing geometry parameter $\kappa = R/L$ and the nondimensional bearing number $\Lambda = 6\mu_0\omega_0/p_0(R/C)^2$ arise, the latter corresponding to the angular velocity $\omega_0 = 2\pi n_0$ of the rotor. Moreover, with regard to transient run-up and coast-down simulations, it is convenient to adopt a characteristic time scale T for the overall problem which does not depend on the rotor speed, giving $\tau = t/T = t/[6\mu_0/p_0(R/C)^2]$. According to Hamrock (1991), the pressurization described by the Reynolds equation results from four basic mechanisms, which are subsequently referred to as Poiseuille flow, Couette flow, fluid expansion, and squeeze flow. With regard to the modeled fluid–structure–rotor interaction, it should be emphasized that the latter can be subdivided into a transient foil structure squeeze flow and a transient rotor journal squeeze flow.

In axial direction, the lubrication gap is open to the atmosphere, imposing ambient pressure $P_0 = 1$ at $Z = \pm 1/2$. With regard to the circumferential direction, however, different concepts can be found in recent literature. A first common approach (see, e.g., San Andrés and Kim, 2010) suggests that the fluid is supplied with ambient pressure through the foil fixation gap (see Figure 2) at a certain angular position $\varphi = \varphi_0$. In this case, the Reynolds equation can be considered on a rectangular domain with four Dirichlet boundaries. A second common approach (see, e.g., Bin Hassan and Bonello, 2017) neglects the foil fixation gap and considers the Reynolds equation on a cylindrical domain with only two Dirichlet boundaries, supposing in addition circumferential periodicity of the fluid properties and of the respective gradients. The present study is based on the second approach with the objective of obtaining generic results which are independent of φ_0.

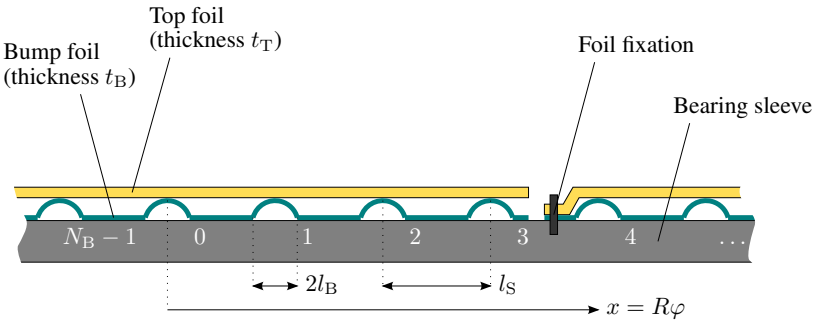

Figure 2. Schematic sketch showing the foil structure configuration (bump foil and top foil) of a typical first generation bump-type GFB.

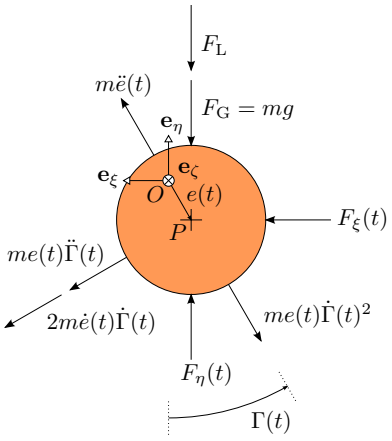

Figure 3. Free body diagram with all the forces acting on the rotor journal.

2.3 Dissipative Foil Structure Model

The schematic sketch in Figure 2 depicts the foil structure configuration which is typically used in first generation bump-type GFBs. It is composed of a thin, corrugated bump foil with N_B bumps (thickness t_B, bump width $2l_\mathrm{B}$, bump distance $l_\mathrm{S} = 2\pi R/N_\mathrm{B}$, Young's modulus E_B, Poisson's ratio ν_B) and a thin, smooth top foil (thickness t_T, Young's modulus E_T, Poisson's ratio ν_T). With the exception of the foil fixation, relative motion and local detachment between the compliant bump foil, the compliant top foil, and the bearing sleeve are possible. Hence, a realistic structure model is supposed to consider not only the foil deformation, but also the energy dissipation caused by dry sliding friction. Earlier experimental works have reported relatively small deformation gradients in axial direction (Ruscitto et al., 1978), confirming that the foil structure can be represented in good approximation by plane 1D models (San Andrés and Kim, 2008) loaded by the axially averaged pressure

$$\overline{P}(\varphi,\tau) = \int_{-\frac{1}{2}}^{+\frac{1}{2}} P(\varphi, Z, \tau)\,\mathrm{d}Z. \tag{5}$$

The classical 2D simple elastic foundation model, sometimes referred to as the Winkler foundation model and firstly applied to GFBs by Heshmat et al. (1983), is not applicable for rotor journal eccentricities $\varepsilon(\tau) \geq 1$ as it predicts non-physical contact at the open bearing edges resulting from the prevailing ambient pressure. However, this issue can be avoided by using a slightly modified 1D simple elastic foundation model respecting the aforementioned assumption of small deformation gradients in axial direction (Baum et al., 2015a; Leister et al., 2016a). In this case, since it is supposed to be uniform along the Z-axis, the elastic deformation $\overline{Q}_\mathrm{e}(\varphi,\tau)$ depends directly on the averaged pressure from Equation (5) and is obtained by the algebraic expression

$$K_\mathrm{W}\overline{Q}_\mathrm{e}(\varphi,\tau) = -\Big[\overline{P}(\varphi,\tau) - 1\Big]. \tag{6}$$

According to Walowit and Anno (1975), the bumps can be approximated by means of a simple beam model, giving the nondimensional foundation stiffness $K_\mathrm{W} = E_\mathrm{B}C/[2(1-{\nu_\mathrm{B}}^2)p_0 l_\mathrm{S}](t_\mathrm{B}/l_\mathrm{B})^3$. Even though the elastic foundation model is completely uncoupled in circumferential direction and does not account for local stiffness variations, no important inaccuracy is expected to result from this simplification (Leister et al., 2016a). Under certain conditions, however, the analytical expression K_W tends to underestimate the real structural stiffness (Larsen et al., 2014). Using Equations (5) and (6), the fluid–structure interaction via film thickness and structure squeeze in Equation (4) is described by

$$\overline{Q}_\mathrm{e}(\varphi,\tau) = -{K_\mathrm{W}}^{-1}\left[\int_{-\frac{1}{2}}^{+\frac{1}{2}} P(\varphi, Z, \tau)\,\mathrm{d}Z - 1\right], \tag{7}$$

$$\overline{Q}'_\mathrm{e}(\varphi,\tau) = -{K_\mathrm{W}}^{-1}\left[\int_{-\frac{1}{2}}^{+\frac{1}{2}} P(\varphi, Z, \tau)\,\mathrm{d}Z\right]' = -{K_\mathrm{W}}^{-1}\underbrace{\int_{-\frac{1}{2}}^{+\frac{1}{2}} P'(\varphi, Z, \tau)\,\mathrm{d}Z}_{(\star)}. \tag{8}$$

Since the Reynolds equation must be solved for the fluid expansion $P'(\varphi, Z, \tau)$ in order to obtain a state-space form, it should be noted that the evaluation of the integral $(\star)$ requires a special treatment upon substitution of Equation (8) into Equation (4). This can be achieved by approximating $(\star)$ using a numerical integration method, which leads to a finite sum of discrete fluid expansion values. The resulting Reynolds equation being linear with respect to the spatially discretized fluid expansion, the state-space form is found by an inverse matrix operation. In this context, it must be stressed that $(\star)$ cannot be neglected if one is interested in a strongly coupled overall model.

As already mentioned, the dominating energy dissipation mechanism is attributed to dry sliding friction. However, according to a proposition by Peng and Carpino (1993), the assumption of equivalent viscous damping reveals to be a useful approximation. Therefore, in addition to the nondimensional stiffness parameter K_W, the nondimensional damping parameter D_W is introduced. Based on the elastic foundation model from Equation (6), an extended viscoelastic foundation model for the deformation $\overline{Q}_\mathrm{v}(\varphi, \tau)$ is stated by the ordinary differential equation (ODE)

$$D_\mathrm{W}\overline{Q}'_\mathrm{v}(\varphi,\tau) + K_\mathrm{W}\overline{Q}_\mathrm{v}(\varphi,\tau) = -\Big[\overline{P}(\varphi,\tau) - 1\Big]. \tag{9}$$

Knowing that Equation (9) is a differential equation rather than an algebraic equation, it is convenient to consider henceforth the foil structure deformation field $\overline{Q}_\mathrm{v}(\varphi, \tau)$ as a state variable with the corresponding state equation

$$\overline{Q}'_\mathrm{v}(\varphi,\tau) = -{D_\mathrm{W}}^{-1}\left[K_\mathrm{W}\overline{Q}_\mathrm{v}(\varphi,\tau) + \int_{-\frac{1}{2}}^{+\frac{1}{2}} P(\varphi, Z, \tau)\,\mathrm{d}Z - 1\right]. \tag{10}$$

Most notably, in contrast to Equation (8) for the elastic model, the integral $(\star)$ does not appear anymore, thus allowing for a simplified evaluation of the Reynolds equation despite the structure model being more comprehensive.

2.4 Turbomachine Rotor Model

As the present study is focused on gaining a basic understanding of energy dissipation inside the bearing, we consider a simple horizontal rigid rotor of mass $2m$ without unbalance, which is symmetrically mounted on two GFBs. In this case, an additional static load $2F_\mathrm{L}$ is equivalent to a modified gravitational acceleration $g + F_\mathrm{L}/m$. Integrating the gas pressure acting on each of the rotor journals, we obtain the nondimensional bearing force vector

$$\mathbf{f}(\tau) = \begin{bmatrix} f_\xi(\tau) \\ f_\eta(\tau) \end{bmatrix}_{\{\mathbf{e}_\xi, \mathbf{e}_\eta\}} = \frac{1}{p_0 R L}\begin{bmatrix} F_\xi(\tau T) \\ F_\eta(\tau T) \end{bmatrix}_{\{\mathbf{e}_\xi, \mathbf{e}_\eta\}} = \int_{-\frac{1}{2}}^{+\frac{1}{2}}\int_0^{2\pi} P(\varphi, Z, \tau)\begin{bmatrix} \sin\varphi \\ \cos\varphi \end{bmatrix}_{\{\mathbf{e}_\xi, \mathbf{e}_\eta\}} \mathrm{d}\varphi\,\mathrm{d}Z. \tag{11}$$

With the nondimensional rotor mass parameter $M = p_0/(36{\mu_0}^2 L)(C/R)^5 m$ and the modified gravity parameter $G = 36{\mu_0}^2/({p_0}^2 R)(R/C)^5(g + F_\mathrm{L}/m)$, the free body diagram in Figure 3 yields the equations of motion

$$\left.\begin{aligned} \varepsilon''(\tau) - \varepsilon(\tau)\gamma'(\tau)^2 - G\cos\gamma(\tau) + \frac{1}{M}\Big[f_\xi(\tau)\sin\gamma(\tau) + f_\eta(\tau)\cos\gamma(\tau)\Big] \\ \varepsilon(\tau)\gamma''(\tau) + 2\varepsilon'(\tau)\gamma'(\tau) + G\sin\gamma(\tau) + \frac{1}{M}\Big[f_\xi(\tau)\cos\gamma(\tau) - f_\eta(\tau)\sin\gamma(\tau)\Big] \end{aligned}\right\} = 0. \tag{12}$$

2.5 State-Space Representation

The domain of the lubrication gap is discretized using a uniform computational grid with $N_\varphi \times N_Z$ grid points. Defining discrete pressure values $P_{i,j}(\tau)$ for the Reynolds equation as well as discrete displacement values $\overline{Q}_i(\tau)$ for the viscoelastic foundation model, we obtain the nondimensional discrete state vector

$$\begin{bmatrix} \mathbf{s}_\mathrm{F}(\tau) \\ \mathbf{s}_\mathrm{S}(\tau) \\ \mathbf{s}_\mathrm{R}(\tau) \end{bmatrix} = \Bigg[\overbrace{P_{0,1}(\tau)\cdots P_{N_\varphi-2,N_Z-2}(\tau)}^{\text{Fluid state } {\mathbf{s}_\mathrm{F}}^\top(\tau)}\ \overbrace{\overline{Q}_0(\tau)\cdots\overline{Q}_{N_\varphi-2}(\tau)}^{\text{Structure state } {\mathbf{s}_\mathrm{S}}^\top(\tau)}\ \overbrace{\varepsilon(\tau)\ \varepsilon'(\tau)\ \gamma(\tau)\ \gamma'(\tau)}^{\text{Rotor state } {\mathbf{s}_\mathrm{R}}^\top(\tau)}\Bigg]^\top \tag{13}$$
$$= \mathbf{s}(\tau) \in \mathbb{R}^{(N_\varphi-1)(N_Z-2)+(N_\varphi-1)+4} = \mathbb{R}^n,$$

which will not contain any structure displacement values if the purely elastic foundation model is considered. For the right-hand side $\mathbf{k}$ of the state equation system, depending on the structure model, we use either Equation (8) or (10). Moreover, a state-space form of Equation (12) is stated for the rotor. With regard to the fluid model, we solve Equation (4) for $P'(\varphi, Z, \tau)$ and discretize all spatial derivatives by means of a finite difference scheme. The bearing number Λ being the bifurcation parameter, we obtain the nonlinear autonomous first-order ODE system

$$\mathbf{s}'(\tau) = \begin{bmatrix} \mathbf{s}_\mathrm{F}(\tau) \\ \mathbf{s}_\mathrm{S}(\tau) \\ \mathbf{s}_\mathrm{R}(\tau) \end{bmatrix}' = \mathbf{k}\left\{\begin{bmatrix} \mathbf{s}_\mathrm{F}(\tau) \\ \mathbf{s}_\mathrm{S}(\tau) \\ \mathbf{s}_\mathrm{R}(\tau) \end{bmatrix}, \Lambda\right\} = \mathbf{k}\Big\{\mathbf{s}(\tau), \Lambda\Big\}, \qquad \mathbf{k}\colon \mathbb{R}^n \times \mathbb{R} \to \mathbb{R}^n. \tag{14}$$

Table 1. Parameters used for the numerical simulations.

Parameter	Symbol	Value
Axial bearing width	L	$38.10\,\mathrm{mm}$
Bearing radius	R	$19.05\,\mathrm{mm}$
Lubrication gap clearance	C	$50\,\mu\mathrm{m}$
Ambient pressure	p_0	$1013.25\,\mathrm{hPa}$
Dynamic viscosity	μ_0	$1.85 \times 10^{-5}\,\mathrm{Ns/m^2}$
Rotational speed	n_0	$36\,000\,\mathrm{min^{-1}}$
Rotor mass	$2m$	$2 \times 185\,\mathrm{g}$
Gravity	g	$9.81\,\mathrm{m/s^2}$
External load	$2F_\mathrm{L}$	$2 \times 20.25\,\mathrm{N}$
Number of bumps	N_B	26
Bump width	$2l_\mathrm{B}$	$2 \times 1.778\,\mathrm{mm}$
Foil thickness	$t_\mathrm{B}, t_\mathrm{T}$	$101.6\,\mu\mathrm{m}$
Young's modulus	$E_\mathrm{B}, E_\mathrm{T}$	$214\,\mathrm{GPa}$
Poisson's number	$\nu_\mathrm{B}, \nu_\mathrm{T}$	0.29

3 Results and Discussion

3.1 Model Parameters

The numerical results presented hereafter are based on data of a typical first generation bump-type GFB, which is referred to in a great number of both experimental and numerical investigations (Ruscitto et al., 1978; Peng and Khonsari, 2004; San Andrés and Kim, 2008), thus allowing the authors to validate their code against the literature. According to the definitions in the preceding sections, a nondimensional parameter set is deduced from the dimensional values in Table 1. In doing so, one must be aware of the uncertainty which might arise from the empirically estimated value $C = 50\,\mu\mathrm{m}$ describing the poorly known lubrication gap clearance (Peng and Khonsari, 2004; Leister et al., 2016b). For the numerical analysis, we use $N_\varphi \times N_Z = 79 \times 7$ grid points, which is sufficient for a grid-independent solution if local stiffness variations of the foil structure are not taken into account (Leister et al., 2016a).

As known from the literature (see, e.g., Thomson, 1996), the equivalent viscous damping can be assessed by opposing the viscoelastic model to a Coulomb friction model (coefficient μ_C) and by equilibrating the respective amounts of energy dissipated during one cycle of a characteristic sinusoidal displacement $\hat{q}\sin(\omega t)$. With the choice of reasonable parameter values and the assumption of a normal force induced by a characteristic pressure p, we obtain the order-of-magnitude estimate

$$D_\mathrm{W} = \overbrace{\frac{4}{\pi}}^{=O(1)} \quad \overbrace{\mu_\mathrm{C}}^{=O(0.1)} \quad \overbrace{\frac{C}{\hat{q}}}^{=O(1)} \quad \overbrace{\frac{\omega_0}{\omega}}^{=O(1)} \quad \overbrace{\frac{p}{p_0}}^{=O(10)} \quad \overbrace{\Lambda^{-1}}^{=O(1)} = O(1). \tag{15}$$

3.2 Stabilization of Stationary Operating Points

In the first part of the analysis, we investigate the capability of frictional energy dissipation to prevent the occurrence of self-excited vibrations in the first place. Mathematically speaking, we are interested in stationary solutions $\mathbf{s}(\tau) = \mathbf{s}_0$ of Equation (14) for which the overall system state remains unchanged as time elapses. For this purpose, the nonlinear algebraic equation system $\mathbf{k}\{\mathbf{s}_0, \Lambda\} = \mathbf{0}$ is solved for $\mathbf{s}_0$ using a Newton–Raphson method with an adequate initial guess. Locally, by virtue of the Hartman–Grobman theorem, the stability of these equilibrium points can be assessed by a consideration of the corresponding linearized problem. Thus, we calculate the eigenvalues λ_i of the numerically approximated Jacobian $\mathbf{J}_\mathbf{k}|_{\mathbf{s}(\tau)=\mathbf{s}_0,\Lambda}$. With the condition $\max_{\lambda_i} \Re(\lambda_i) < 0$ for asymptotic stability, the critical bearing number $\Lambda = \Lambda_\mathrm{c}$ can be estimated using a numerical continuation method. From a practical point of view, the existence of a stability threshold suggests that no stable stationary operating point of the GFB rotor system is possible anymore if some critical rotor speed is exceeded.

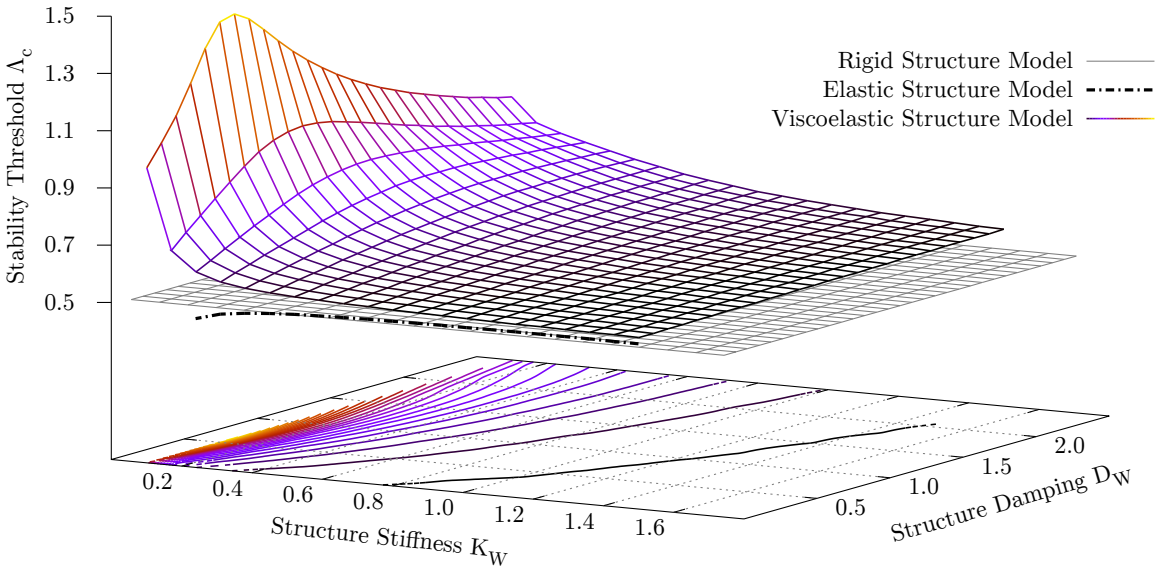

Figure 4. Stability diagram showing the critical bearing number depending on foil structure stiffness and damping.

In the stability diagram in Figure 4, the black chain-dotted line visualizes the critical bearing number for the elastic structure model as a function of the structure stiffness K_W. As a reference, the gray surface indicates the critical bearing number which is found for a rigid bearing with the same parameters but without any structural deformation. When comparing the results found with the elastic model and the results found with the rigid model, a slightly stabilizing effect due to the foil structure deformation can be observed for stiffnesses $K_\mathrm{W} > 0.4$, which is in accordance with earlier works by the authors (Baum et al., 2015a; Leister et al., 2016b). On the other hand, if the stiffness is excessively low, the overall system is destabilized to such an extent that no stable equilibrium point at all can be found.

For the viscoelastic model, the multicolored surface in Figure 4 visualizes the critical bearing number as a function of the structure stiffness K_W and the structure damping D_W, both of them influencing the eigenvalues. In contrast to the elastic model, much larger critical bearing numbers are predicted, in particular for low stiffnesses. As shown in the diagram, a specific optimum damping value which maximizes the critical bearing number is associated to each stiffness value. When the stiffness is increased, the optimum damping is also shifted toward higher values.

Thus, we conclude that energy dissipation within the foil structure has the potential to stabilize stationary operating points of the GFB rotor system and, if the dissipation rate is chosen appropriately, to prevent the occurrence of undesirable self-excited vibrations in the first place.

3.3 Nonlinear Dynamic Response of the System during Run-Up and Coast-Down

Despite the stabilizing effect of frictional energy dissipation, the occurrence of self-excited vibrations can only be shifted toward higher rotational speeds and is never completely avoidable. In order to gain a basic understanding of the dynamic response of the GFB rotor system, a typical machine run-up and coast-down scenario is simulated in this part of the analysis. According to the first plot in Figure 5, the rotational speed is varied linearly during $\tau_\mathrm{max} = 50\,000$ ($t_\mathrm{max} = 50\,\mathrm{s}$) from $\Lambda_1 = 0.500$ ($n_1 = 30\,000\,\mathrm{min}^{-1}$) to $\Lambda_2 = 0.833$ ($n_2 = 50\,000\,\mathrm{min}^{-1}$) and back. The numerical time integration of Equation (14) is performed using a trapezoidal-type scheme in order to avoid numerical damping.

The second and the third plot in Figure 5 show the horizontal position of the rotor journal $\xi(\tau)$ as a red signal envelope curve and the vertical position of the rotor journal $\eta(\tau)$ as a blue signal envelope curve. In each of the plots, the solid lines correspond to the viscoelastic structure model and the chain-dotted lines correspond to the rigid structure model. Beyond the critical bearing number, no further stationary solution is stable and the onset of self-excited vibrations can be observed. In accordance with the eigenvalue analysis above, the critical bearing number is significantly higher for the viscoelastic model compared to the rigid model. During the coast-down, the self-excited vibrations collapse only at a subcritical bearing number and the resulting asymmetry of the curves suggests that a certain range of bearing numbers exists where both stationary and periodic solutions are stable. This

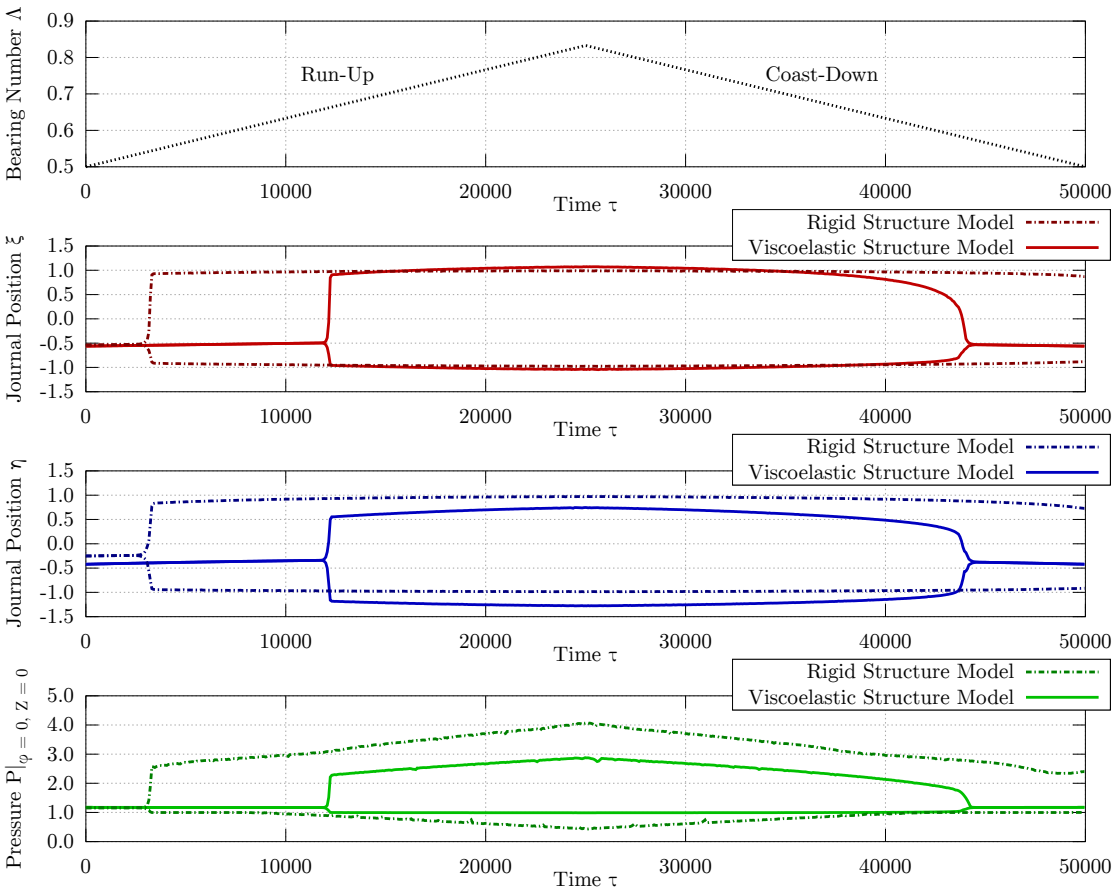

Figure 5. Signal envelopes of rotor journal position and fluid pressure during run-up and coast-down.

is a characteristic property of dynamic systems in which a subcritical Poincaré–Andronov–Hopf bifurcation and a subsequent fold bifurcation of cycles occur (Baum et al., 2015a,b). Most notably, the vertical rotor journal vibrations with the viscoelastic model exhibit smaller amplitudes than the rigid model predicts. Moreover, the absolute positions are shifted vertically because of the foil structure deformation, which allows for positions with $|\xi(\tau)| \geq 1$ and/or $|\eta(\tau)| \geq 1$.

The fourth plot in Figure 5 shows, at an exemplary point, the pressure $P(0, 0, \tau)$ as a green signal envelope curve. The arising oscillation is similar to the rotor journal position oscillations. It should be noted that each of the discrete pressure values could be considered as a vibrating subsystem. For the viscoelastic model, the pressure peaks are significantly lower than for the rigid model as a result of the foil structure deformation. Most notably, in contrast to the rigid model, this result shows that almost no underpressure with $P(\varphi, Z, \tau) < P_0$ is predicted by the viscoelastic model. Assuming the top foil to be lifted up until ambient pressure is reached, underpressure is forbidden in most of the available literature using a boundary condition originally proposed by Heshmat et al. (1983). However, according to the present investigation, this assumption seems to be redundant if an appropriate structure model is utilized, knowing that the top foil lift-off could also be limited by a counteracting structural stiffness.

Altogether, we conclude that frictional energy dissipation does not only increase the critical bearing number but has also the potential to reduce the amplitudes of self-excited vibrations if these cannot be avoided.

3.4 Amplitude Reduction of Self-Excited Vibrations

In the last part of the analysis, we investigate the aforementioned capability of frictional energy dissipation to reduce the amplitudes of self-excited vibrations if their occurrence cannot be prevented in the first place. Thus, we are now interested in limit cycles, i.e., periodic solutions $\mathbf{s}(\tau) = \mathbf{s}_\mathrm{p}(\tau)$ of Equation (14) which verify the conditions

$$\mathbf{s}_\mathrm{p}{}'(\tau) = \mathbf{k}\Big\{\mathbf{s}_\mathrm{p}(\tau), \Lambda\Big\}, \qquad \mathbf{s}_\mathrm{p}(\tau) = \mathbf{s}_\mathrm{p}(\tau + \mathcal{T}). \tag{16}$$

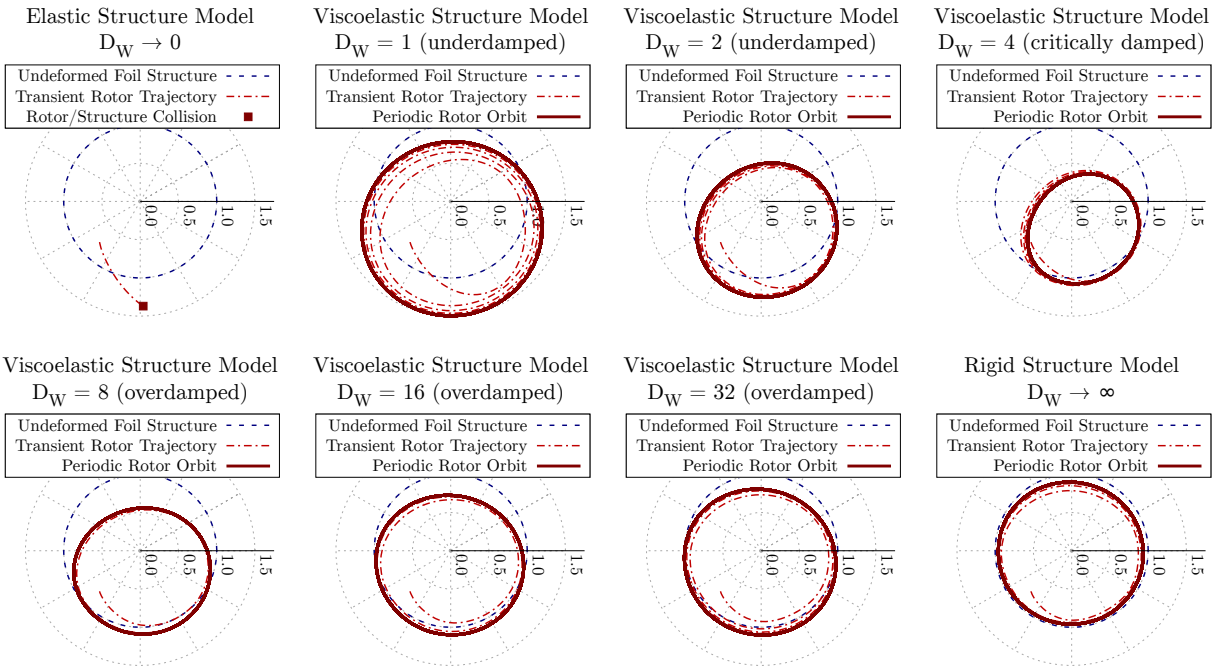

Figure 6. Periodic rotor journal orbits (self-excited vibrations) with increasing foil structure damping.

Choosing a moderate stiffness $K_\mathrm{W} = 1$ and maintaining the rotational speed $\Lambda_0 = 0.600$ ($n_0 = 36\,000\,\mathrm{min}^{-1}$), the influence of a varying damping parameter D_W is investigated in Figure 6. The chain-dotted red lines show rotor journal trajectories, which result in stable periodic orbits highlighted by thicker solid red lines. With the elastic structure model, no stable periodic orbit can be observed in the numerical simulation because the rotor journal is predicted to collide with the excessively deformed top foil. However, stable periodic orbits can be reproduced as expected when considering the viscoelastic structure model. With weak damping $D_\mathrm{W} < 4$, the arising vibrations exhibit relatively large amplitudes with rotor journal eccentricities $\varepsilon(\tau) > 1$. These amplitudes are reduced with increasing damping coefficient, the optimum being equal to the critical damping $D_\mathrm{W} \approx 4$, which has already been identified with regard to the stability of stationary equilibrium points. With strong damping $D_\mathrm{W} > 4$, the rotor journal eccentricities fall back to $\varepsilon(\tau) \approx 1$. In accordance with a proposition by Le Lez et al. (2007), we conclude that there is an optimum damping which ensures to dissipate the maximum energy possible per cycle.

In Figure 7, some of the periodic solutions are compared in the frequency domain by means of an FFT analysis, yielding characteristic subsynchronous whirling frequencies with $2\pi/\mathcal{T} \approx \Lambda/2$. According to a heuristic explanation given by Genta (2009), the observed whirling speeds are directly correlated with the circumferential fluid velocity, which is the superposition of a Poiseuille flow and a Couette flow. Dominated by the triangular velocity profile of the Couette flow, the average circumferential fluid velocity is found to be approximately equal to half the peripheral rotor journal speed. Due to a decelerating influence of the Poiseuille flow, which is typically growing with increasing fluid film thickness, whirling motions at rather small eccentricities may actually occur with distinctly lower whirling speeds. In accordance with this expectation, the results of the FFT analysis reveal that not only the amplitudes but also the frequencies are minimized when considering the critically damped viscoelastic structure model. Altogether, it can be concluded that energy dissipation strongly affects subsynchronous whirling phenomena and thus must be considered carefully in realistic simulations.

4 Conclusion and Perspective

The nonlinear GFB rotor model presented in this paper has been developed with the aim of capturing the true coupled nature of fluid–structure–rotor interaction phenomena. As the present study is focused on gaining a basic understanding of frictional energy dissipation inside the bearing, a rather simple structure model based on a viscoelastic foundation is utilized. It has been shown that damping stabilizes stationary operating points and that the occurrence of self-excited vibrations may be prevented if an adequate dissipation rate is ensured. Moreover, it has been shown that vibrational amplitudes can be reduced significantly by means of frictional energy dissipation. Summing up all results, frictional energy dissipation proves to be of crucial importance with regard to the reduction or prevention of undesirable self-excited vibrations in GFB rotor systems.

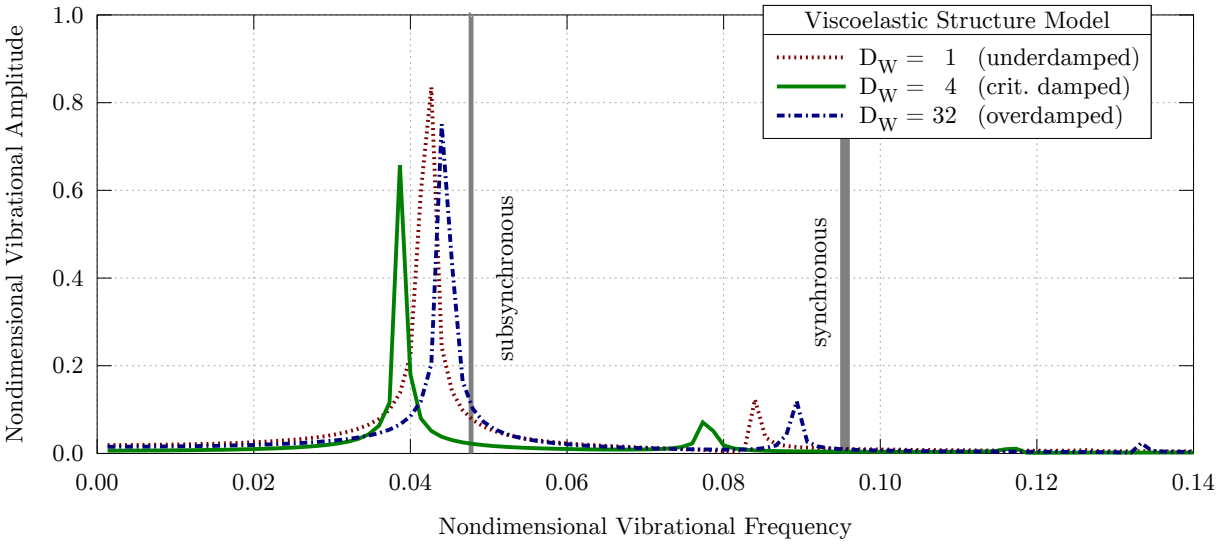

Figure 7. FFT analysis of an underdamped, a critically damped, and an overdamped GFB rotor system.

Future work will aim at the development of a more sophisticated dry sliding friction model considering stick–slip transitions and interaction mechanisms between the bumps. Moreover, the fluid model will be extended with regard to thermal effects and more realistic rotor models will be integrated into the simulation, knowing that many practical issues caused by subsynchronous vibrations are directly related to heavy loading conditions and rotor unbalance.

References

Baum, C.; Hetzler, H.; Seemann, W.: On the stability of balanced rigid rotors in air foil bearings. In: *Proceedings of the SIRM 2015*, Magdeburg, Germany (2015a).

Baum, C.; Leister, T.; Seemann, W.: Foil air bearing rotor interaction – Bifurcation analysis of a Laval rotor. In: *Proceedings of the EUROMECH Colloquium 573*, Lyon, France (2015b).

Bin Hassan, M. F.; Bonello, P.: A neural network identification technique for a foil-air bearing under variable speed conditions and its application to unbalance response analysis. *Journal of Tribology*, 139, 2, (2017).

Bonello, P.; Pham, H. M.: The efficient computation of the nonlinear dynamic response of a foil-air bearing rotor system. *Journal of Sound and Vibration*, 333, 15, (2014), 3459–3478.

Bou-Saïd, B.; Grau, G.; Iordanoff, I.: On nonlinear rotor dynamic effects of aerodynamic bearings with simple flexible rotors. *Journal of Engineering for Gas Turbines and Power*, 130, 1, (2008).

Genta, G.: *Vibration Dynamics and Control*. Springer, New York, United States of America (2009).

Hamrock, B. J.: *Fundamentals of Fluid Film Lubrication (NASA Reference Publication 1255)*. National Aeronautics and Space Administration, United States of America (1991).

Heshmat, H.; Walowit, J. A.; Pinkus, O.: Analysis of gas-lubricated foil journal bearings. *Journal of Lubrication Technology*, 105, 4, (1983), 647–655.

Hoffmann, R.; Pronobis, T.; Liebich, R.: Non-linear stability analysis of a modified gas foil bearing structure. In: *Proceedings of the 9th IFToMM International Conference on Rotor Dynamics*, Milan, Italy (2014).

Howard, S. A.: Rotordynamics and design methods of an oil-free turbocharger. Tech. Rep. NASA CR-208689, National Aeronautics and Space Administration, United States of America (1999).

Howard, S. A.; Bruckner, R. J.; DellaCorte, C.; Radil, K. C.: Gas foil bearing technology advancements for closed Brayton cycle turbines. Tech. Rep. NASA TM-214470, National Aeronautics and Space Administration, United States of America (2007).

Howard, S. A.; Bruckner, R. J.; Radil, K. C.: Advancements toward oil-free rotorcraft propulsion. Tech. Rep. NASA TM-216094, National Aeronautics and Space Administration, United States of America (2010).

Howard, S. A.; DellaCorte, C.; Valco, M. J.; Prahl, J. M.; Heshmat, H.: Dynamic stiffness and damping characteristics of a high-temperature air foil journal bearing. *Tribology Transactions*, 44, 4, (2001), 657–663.

Larsen, J. S.; Varela, A. C.; Santos, I. F.: Numerical and experimental investigation of bump foil mechanical behaviour. *Tribology International*, 74, (2014), 46–56.

Le Lez, S.; Arghir, M.; Frêne, J.: Static and dynamic characterization of a bump-type foil bearing structure. *Journal of Tribology*, 129, 1, (2007), 75–83.

Leister, T.; Baum, C.; Seemann, W.: Computational analysis of foil air journal bearings using a runtime-efficient segmented foil model. In: *Proceedings of the ISROMAC 2016*, Honolulu, United States of America (2016a).

Leister, T.; Baum, C.; Seemann, W.: Sensitivity of computational rotor dynamics towards the empirically estimated lubrication gap clearance of foil air journal bearings. *Proc. Appl. Math. Mech.*, 16, 1, (2016b), 285–286.

Peng, J.-P.; Carpino, M.: Calculation of stiffness and damping coefficients for elastically supported gas foil bearings. *Journal of Tribology*, 115, 1, (1993), 20–27.

Peng, Z. C.; Khonsari, M. M.: Hydrodynamic analysis of compliant foil bearings with compressible air flow. *Journal of Tribology*, 126, 3, (2004), 542–546.

Reynolds, O.: On the theory of lubrication and its application to Mr. Beauchamp Tower's experiments, including an experimental determination of the viscosity of olive oil. *Philosophical Transactions of the Royal Society of London*, 177, (1886), 157–234.

Ruscitto, D.; McCormick, J.; Gray, S.: Hydrodynamic air lubricated compliant surface bearing for an automotive gas turbine engine, I – Journal bearing performance. Tech. Rep. NASA CR-135368, National Aeronautics and Space Administration, United States of America (1978).

San Andrés, L.; Kim, T. H.: Analysis of gas foil bearings integrating FE top foil models. *Tribology International*, 42, 1, (2008), 111–120.

San Andrés, L.; Kim, T. H.: Thermohydrodynamic analysis of bump type gas foil bearings: A model anchored to test data. *Journal of Engineering for Gas Turbines and Power*, 132, 4, (2010).

Szeri, A. Z.: *Fluid film lubrication*. Cambridge University Press, Cambridge, United Kingdom, 2nd edn. (2010).

Thomson, W.: *Theory of Vibration with Applications*. CRC Press, Boca Raton, United States of America, 4th edn. (1996).

Walowit, J. A.; Anno, J. N.: *Modern developments in lubrication mechanics*. Applied Science Publishers, London, United Kingdom (1975).

Address: Institute of Engineering Mechanics, Karlsruhe Institute of Technology, Kaiserstr. 10, D-76131 Karlsruhe
e-mail: {tim.leister, christoph.baum, wolfgang.seemann}@kit.edu